IMPACT OF SUCTION/INJECTION AND HEAT TRANSFER ON UNSTEADY MHD FLOW OVER A STRETCHABLE ROTATING DISK

K.V. PRASAD[†], H. VAIDYA[†], O. D. MAKINDE[‡],
K. VAJRAVELU[§] and V. RAMANJINI[†]

† *Department of Mathematics, VSK University, Vinayaka Nagar, Ballari – 583105, Karnataka, India.*
Corresponding Author: hanumeshvaidya@gmail.com
‡ *Faculty of Military Science, Stellenbosch University, Private Bag X2, Saldanha 7395, South Africa*
§ *Department of Mathematics, University of Central Florida, Orlando, FL 32816, USA*

***Abstract*– In this article, the unsteady magnetohydrodynamic two-dimensional boundary layer flow and heat transfer over a stretchable rotating disk with mass suction/injection is investigated. Temperature-dependent physical properties and convective boundary conditions are taken into account. The governing coupled nonlinear partial differential equations are transformed into a system of ordinary differential equations by adopting the well-known similarity transformations. Further, the solutions are obtained through the semi-analytical method called an Optimal Homotopy Analysis Method (OHAM). The obtained results are discussed graphically to predict the features of the involved key parameters which are monitoring the flow model. The skin friction coefficient and Nusselt number are also examined. The validation of the present work is verified with the earlier published results and is found to be in excellent agreement. It is noticed that an increase in the viscosity parameter, unsteady parameter, Hartmann number leads to decay in momentum boundary layer thickness, and the inverse trend is observed in the case of the temperature profile.**

***Keywords*— Unsteady flow, Variable fluid proper ties, Rotating disk, Mass suction/ injection, OHAM.**

I. INTRODUCTION

In recent years, numerous researchers analyzed the suction and injection process over different geometries because of its vast applications in engineering and technological domains such as thrust bearing design, radial diffusers, thermal oil recovery, and many others. Erickson *et al*. (1966) considered the stretchable surface to examine the impact of suction/ injection on the flow field. Fox *et al.* (1968) contributed similar work for uniform surface velocity and temperature. Gupta and Gupta (1977) continued the work of Erickson *et al*. (1966) by making the changes in the speed of the surface. Chen and Char (1988) explored the impacts of suction and injection on the heat transfer attributes of a continuous, linearly elastic sheet for both the variations of power-law surface temperature and heat flux. The examination of the behavior of suction /injection on the flow and heat transfer with a power-law stretching sheet was reported by Ali (1995); Cortel (2005) added the permeability to the linear stretching sheet and analyzed the internal heat generation/ absorption nature on the flow pattern. Prasad and Vajravelu (2009) investigated the behavior of power-law fluids over a flat surface in the presence of a magnetic field and suction/injection parameter. Khan *et al.* (2018) utilized OHAM to obtain the numerical results of an unsteady Casson fluid past a stretching sheet in the presence of mass suction/injection. Further, Maleki *et al.* (2019a, 2019b) considered pseudoplastic non-Newtonian fluid over a permeable elastic surface and studied effects of suction or injection. Recently, Shakiba and Rahimi (2019) used the vertical cylindrical surface geometry and reported the impact of suction/ injection on the flow of nanofluid. Wakif *et al*. (2018) analyzed the combined effects of the thermal radiation and a transverse magnetic field on the unsteady natural convection Couette- flow in Cu-water nanofluid numerically. Some recent works on MHD fluid flow and heat transfer with different geometries were extensively studied by Qasim *et al*. (2019a, 2019b, 2019c), Wakif *et al.* (2019a,2019b) and Amanullah *et al*. (2018).

In addition to flow over a stretching sheet, the flow induced by rotating disk has also got several applications in the science and Technological industry such as jet motors, electronic devices, and rotational air cleaners, computer storage devices, rotating machinery, medical equipment, spin coating, and many others. Von Karman (1921) introduced the method to solve the problem of the Navier-Stokes equations for a rotating disk of infinite radius. Cochran (1931) extended the work of Von Karman (1921) using the numerical integration method and obtained more accurate results. Kuiken (1971) reported the impact of the blowing through a porous rotating disk; Watson *et al.* (1979, 1985); examined the unsteady flow over a porous rotating disk and discussed the deceleration case. Takhar *et al*. (1995) investigated the unsteady flow of a micropolar fluid due to a decelerating porous rotating disk with suction/ injection. Fang and Tao (2012) visited the work of Watson *et al.* (1979) examined the unsteady flow induced by a stretchable rotating disk, and obtained a physically feasible solution branch. Rashidi *et al*. (2013) discussed the unsteady MHD flow over a rotating surface in the presence of an artificial neural network. Hobiny *et al*. (2015) reported numerical solution via a shooting method for unsteady viscous flow due to a nonlinear stretchable rotating disk. Furthermore, Turkyilmazoglu (2018) scrutinized the unsteady flow and heat characteristics over a vertically moving rotating disk. Prasad *et al*. (2019) investigated the MHD Casson nanofluid flow over a rotating disk with heat source/sink and slip effects.

All the above researchers analyzed the flow and heat transfer characteristics over the disk/sheet by considering the constant thermophysical properties. However, several researchers (Vajravelu *et al.*, 2013; Prasad *et al.*, 2017a; 2017b) considered variable thermophysical properties. Here, the ambient fluid may change with temperature, namely viscosity and thermal conductivity of the fluid. Effects of Hall current and variable fluid properties on MHD flow due to a rotating porous disk was reported by Abdul Maleque and Abdus Sattar (2005), Fresteri and Osalusi (2007) discussed the MHD slip flow over a porous rotating disk in the presence of variable fluid properties. Rashidi *et al.* (2014) investigated the MHD slip flow over a porous rotating disk with variable fluid properties. Vajravelu *et al.* (2016) studied the effects of variable transport properties and velocity-temperature slips of MHD squeeze flow between parallel disks with transpiration using OHAM. Recently, Prasad *et al.* (2018) scrutinized the effects of variable viscosity and variable thermal conductivity on the Casson fluid flow past a vertical stretching sheet with transpiration.

To the author's best knowledge, no combined work has been made earlier to study the unsteady MHD convective boundary layer flow and heat transfer over a stretchable rotating disk in the presence of mass suction/ injection. Moreover, the impact of viscous dissipation and variable fluid properties such as variable viscosity and variable thermal conductivity are considered. The solutions are obtained via Optimal Homotopy Analysis Method (Liao, 2010 and Von Garder, 2019). An important finding, for instance, the unsteady parameter; viscosity parameter, and Hartmann number squeeze the momentum boundary layer thickness, which complements the existing results in the literature.

II. MATHEMATICAL FORMULATION

Consider an unsteady two dimensional viscous incompressible axially symmetric convective flows and heat transfer over a stretchable rotating disk, which has an angular velocity varying with time ($\Omega/(1-\beta t)$) in the presence of external magnetic field along the *z*-axis. The physical model of the rotating disk is presented in Fig. 1.

Under these assumptions, governing equations for continuity, momentum and energy in cylindrical coordinates as follows,

$$\frac{1}{r}\frac{\partial}{\partial r}(ru_r)+\frac{\partial u_z}{\partial r}=0 \tag{1}$$

$$\frac{\partial u_r}{\partial t}+u_r\frac{\partial u_r}{\partial r}+u_z\frac{\partial u_r}{\partial z}-\frac{u_\theta^2}{r}=\frac{1}{\rho_\infty}\frac{\partial}{\partial z}\left(\mu(T)\frac{\partial u_r}{\partial z}\right)-\frac{\sigma B^2}{\rho_\infty}u_r \tag{2}$$

$$\frac{\partial u_\theta}{\partial t}+u_r\frac{\partial u_\theta}{\partial r}+u_z\frac{\partial u_\theta}{\partial z}-\frac{u_r u_\theta}{r}=\frac{1}{\rho_\infty}\frac{\partial}{\partial z}\left(\mu(T)\frac{\partial u_\theta}{\partial z}\right)-\frac{\sigma B^2}{\rho_\infty}u_\theta \tag{3}$$

$$\frac{\partial T}{\partial t}+u_r\frac{\partial T}{\partial r}+u_z\frac{\partial T}{\partial z}=\frac{1}{\rho_\infty C_p}\frac{\partial}{\partial z}\left(K(T)\frac{\partial T}{\partial z}\right)+\frac{1}{\rho_\infty C_p}\mu(T)\left(\left(\frac{\partial u_r}{\partial z}\right)^2+\left(\frac{\partial u_\theta}{\partial z}\right)^2\right) \tag{4}$$

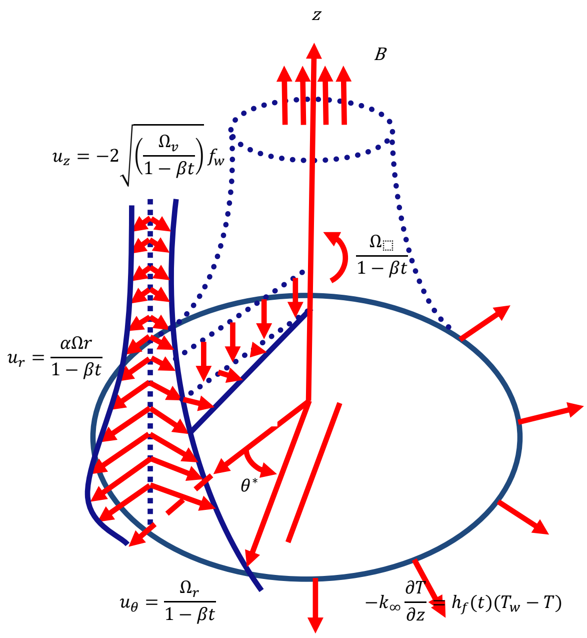

Fig. 1: Geometry of the physical model.

where (u_r, u_θ, u_z) are the velocity components in the direction of the cylindrical coordinate system (r,θ^*,z), t is the time, ρ_∞ is the density of the fluid, σ is the electrical conductivity, $B(t)=B_0(1-\beta t)^{-1/2}$is the special form of magnetic field imposed along the z-axis, C_p is the specific heat at constant pressure. Further, it is assumed that the thermo-physical transport properties of the fluid are constant except for the fluid viscosity $\mu(T)$ and thermal conductivity $K(T)$ which varies as a function of temperature in the following forms:

$$\mu(T)=\mu_\infty[1+\gamma(T-T_\infty)]^{-1}, i.e.\, \mu^{-1}=a(T-T_r) \tag{5}$$

where $a=\gamma/\mu_\infty$ and $T_r=T_\infty-1/\gamma$ are constants and their values depend on the reference state and thermal property of the fluid. In general, $a>0$ indicates the liquid and $a<0$ indicates the gases.

$$K(T)=k_\infty[1+\varepsilon\Delta T^{-1}(T-T_\infty)] \tag{6}$$

where $\mu(T)$, $K(T)$, μ_∞ and k_∞ are respectively called variable fluid viscosity, variable thermal conductivity, coefficient of viscosity of the fluid and thermal conductivity of the fluid far away from the disk, γ is the thermal property of the fluid, $\varepsilon=(k_w-k_\infty)/k_\infty$ is a variable thermal conductivity parameter, ΔT=T_w-T_∞ is the temperature difference, k_w is the thermal conductivity, $\theta_r=(T_r-T_\infty)/\Delta T=-1/(\gamma\Delta T)$ is the fluid viscosity parameter, which is negative for liquids and positive for gases (for more details see Prasad *et al.*, 2017a). Using Eqns. (5) and (6) in (2) to (4) reduces to,

$$\frac{\partial u_r}{\partial t}+u_r\frac{\partial u_r}{\partial r}+u_z\frac{\partial u_r}{\partial z}-\frac{u_\theta^2}{r}+\frac{\sigma B^2}{\rho_\infty}u_r=\frac{1}{\rho_\infty}\frac{\partial}{\partial z}\left(\frac{\mu_\infty}{1+\gamma(T-T_\infty)}\frac{\partial u_r}{\partial z}\right) \tag{7}$$

$$\frac{\partial u_\theta}{\partial t}+u_r\frac{\partial u_\theta}{\partial r}+u_z\frac{\partial u_\theta}{\partial z}-\frac{u_r u_\theta}{r}+\frac{\sigma B^2}{\rho_\infty}u_\theta=\frac{1}{\rho_\infty}\frac{\partial}{\partial z}\left(\frac{\mu_\infty}{1+\gamma(T-T_\infty)}\frac{\partial u_\theta}{\partial z}\right) \tag{8}$$

$$\frac{\partial T}{\partial t}+u_r\frac{\partial T}{\partial r}+u_z\frac{\partial T}{\partial z}=$$

$$\frac{1}{\rho_\infty C_p}\frac{\partial}{\partial z}\left(k_\infty\left(1+\frac{\varepsilon}{\Delta T}(T-T_\infty)\right)\frac{\partial T}{\partial z}\right)+$$
$$\frac{1}{\rho_\infty C_p}\frac{\mu_\infty}{1+\gamma(T-T_\infty)}\left(\left(\frac{\partial u_r}{\partial z}\right)^2+\left(\frac{\partial u_\theta}{\partial z}\right)^2\right) \quad (9)$$

Appropriate boundary conditions are,

$$u_r = \alpha\Omega r/(1-\beta t),\, u_\theta = \Omega r/(1-\beta t)$$
$$u_z = -2\sqrt{\Omega v(1-\beta t)}f_w,$$
$$-k_\infty\frac{\partial T}{\partial z} = h_f(t)(T_w - T) \quad \text{at} \quad z=0$$
$$u_r \to 0, u_\theta \to 0, T \to T_\infty \quad \text{at} \quad z \to \infty. \quad (10)$$

where $\alpha = b/\Omega$ is the disk stretching parameter, $h_f(t) = h_f(1-\beta t)^{-1/2}$ is the special form of heat transfer coefficient. Now the following similarity transformations are introduced to reduce the governing equations into dimensionless form (for more details see Fang and Tao, 2012).

$$u_r = u_w(=\Omega r/(1-\beta t))f'(\eta),$$
$$u_\theta = \Omega r/(1-\beta t)g(\eta),$$
$$u_z = -2\sqrt{\Omega v_\infty/(1-\beta t)}f(\eta),$$
$$\theta(\eta) = (T-T_\infty)/(T_w-T_\infty)(=\Omega r/(1-\beta t))$$
$$\eta = \sqrt{\Omega/v_\infty(1-\beta t)}z,\, B^2 = B_0^2/(1-\beta t) \quad (11)$$

Using Eq. (11), Eq. (1) is automatically satisfied and Eqns. (7) to (10) takes the self-similar form,

$$(f''(1-\theta/\theta_r)^{-1})' + g^2 + 2ff'' - f'^2 -$$
$$-S(f' + (1/2)\eta f'') - Mnf' = 0 \quad (12)$$
$$(g'(1-\theta/\theta_r)^{-1})' + 2fg' - 2f'g -$$
$$-S(g + (1/2)\eta g') - Mng = 0 \quad (13)$$
$$((1+\varepsilon\theta)\theta')' + \Pr Ec\,(1-\theta/\theta_r)^{-1}(f''^2 + g'^2) +$$
$$+2\Pr f\theta' - \Pr f'\theta - \Pr S\,(\theta + (1/2)\eta\theta') = 0, (14)$$
$$f(0) = f_w, f'(0) = \alpha, g(0) = 1, \theta'(0) = -\delta(1-\theta(0)),$$
$$f'(\infty) \to 0, g(\infty) \to 0, \theta(\infty) \to 0, \quad (15)$$

here prime denotes derivative with respect to η, $(f(\eta)$, $f'^{(\eta)}, g(\eta), \theta(\eta))$ are respectively called the axial, radial, tangential velocity profiles and temperature profile, $Mn = \sigma B^2/\rho_\infty\Omega$, $\Pr = \mu_\infty C_p/k_\infty$, $Ec = u_w\Omega/cC_p$ and$\delta = h_f/k_\infty\sqrt{v_\infty/\Omega}$ are respectively called Hartmann number, Prandtl number, Eckert number and Biot number, $S = \beta/\Omega$ is called unsteady parameter where $S > 0$ corresponds disk acceleration and $S < 0$ corresponds disk deceleration, f_w is called mass transfer parameter where $f_w > 0$ indicate mass suction and $f_w < 0$ indicate mass injection. Important physical parameters for engineering interest are local skin friction and Nusselt number given by,

$$C_f = (1-\beta t)^2/\rho_\infty(r\Omega)^2\sqrt{(\tau_{zr})^2 + (\tau_{z\theta})^2}$$
$$Nu = rq_w/k_\infty(T_w - T_\infty), \quad (16)$$

where τ_{zr} and $\tau_{z\theta}$ re called radial and tangential shear stress at the surface of the disk and q_w is the heat flux which are defined as follow,

$$\tau_{zr} = \mu(T)\left(\frac{\partial u_r}{\partial z}\right)\Big|_{z=0},\, \tau_{z\theta} = \mu(T)\left(\frac{\partial u_\theta}{\partial z}\right)\Big|_{z=0},$$
$$q_w = -K(T)\left(\frac{\partial T}{\partial z}\right)\Big|_{z=0}.$$

Substituting Eqn. (11) in (16) we get,

$$C_f(Re)^{1/2} = (1-\theta/\theta_r)^{-1}\left[(f''(0))^2 + (g'(0))^2\right]^{1/2}$$
$$Nu(Re)^{-1/2} = -(1+\varepsilon\theta)\theta'(0), \quad (17)$$

wkere $Re = \Omega r^2/v(1-\beta t)$ is the Reynolds number.

III. METHOD OF SOLUTION

To obtain the appropriate solutions for the system of coupled highly nonlinear ordinary differential equations (12)-(14) with boundary conditions (15), we adopt the following semi-analytical technique such as Optimal Homotopy Analysis Method (OHAM). Now we can pick the initial guesses for velocity and temperature in line with given the boundary conditions,

$$f_0(\eta) = f_w + \alpha e^{-\eta}, g_0(\eta) = e^{-\eta},\, \theta_0(\eta) = \frac{\delta}{1+\delta}e^{-\eta} \quad (18)$$

and appropriate linear operators for the governing problems are defined as follow,

$$L_f = \frac{d^3}{d\eta^3} + \frac{d^2}{d\eta^2}, L_g = \frac{d^2}{d\eta^2} - g, L_\theta = \frac{d^2}{d\eta^2} - \theta. \quad (19)$$

Convergence control parameters for optimal values: The optimal values of the convergence of solution series depend upon the auxiliary parameters known as convergence control parameters such as $(\bar{h}_f, \bar{h}_g, \bar{h}_\theta) \neq 0$ and these can be used to control the convergence region and the rate of convergence of the series solution. Therefore, the optimal homotopy analysis method (OHAM) gives an appropriate convergent solution. To get the optimized values of $\bar{h}_f$, $\bar{h}_g$ and $\bar{h}_\theta$, we have to use the concept of minimization by defining the averaged squared residual errors,

$$\bar{E}_P^f(\bar{h}_f) = \int_0^1\left(N_f\sum_{y=0}^{P}\hat{f}_y(\eta)\right)^2 d\eta,$$
$$\bar{E}_P^g(\bar{h}_g) = \int_0^1\left(N_g\sum_{y=0}^{P}\hat{g}_y(\eta)\right)^2 d\eta, \quad (20)$$
$$\bar{E}_P^\theta(\bar{h}_\theta) = \int_0^1\left(N_\theta\sum_{y=0}^{P}\hat{\theta}_y(\eta)\right)^2 d\eta.$$

The pioneering work of individual and total averaged squared residual errors are introduced by Liao (2010) and which can be mathematically expressed as E_n^f, E_n^g, E_n^θ and $E_n^t = E_n^f + E_n^g + E_n^\theta$. It is clearly verified that the averaged and total squared residual errors gradually decrease as the order of the approximation rises, which confirms that OHAM exists successfully (See Table1 and Table.2).

Table 1: Individual average residual errors as a function of the number of iterations when parameters are fixed at $= Mn = S = 1, \delta = Ec = 0.5, \Pr = 0.72, f_w = \varepsilon = 0.1, \theta_r = -10$.

p	$\bar{E}_P^f$	$\bar{E}_P^g$	$\bar{E}_P^\theta$	CPU time (s)
2	$5.29\text{x}10^{-4}$	$6.78\text{x}10^{-3}$	$2.48\text{x}10^{-4}$	11.6205
4	$8.34\text{x}10^{-6}$	$1.42\text{x}10^{-4}$	$3.67\text{x}10^{-5}$	54.5011
6	$1.91\text{x}10^{-6}$	$6.26\text{x}10^{-6}$	$7.47\text{x}10^{-6}$	263.945
8	$3.44\text{x}10^{-7}$	$3.51\text{x}10^{-7}$	$8.53\text{x}10^{-7}$	790.305
10	$5.37\text{x}10^{-8}$	$1.86\text{x}10^{-8}$	$1.53\text{x}10^{-7}$	2169.01
12	$7.67\text{x}10^{-9}$	$5.81\text{x}10^{-10}$	$4.27\text{x}10^{-8}$	4040.75
14	$1.07\text{x}10^{-9}$	$3.53\text{x}10^{-11}$	$1.98\text{x}10^{-8}$	8944.68

Table 2: Total squared residual errors and conver gence control parameters for different approximation p.

p	$-\bar{h}_f$	$-\bar{h}_g$	$-\bar{h}_\theta$	E_p^t	CPU time (s)
2	0.8991	0.9676	1.086	2.06×10^{-2}	11.6205
4	0.9237	0.9480	1.050	1.39×10^{-4}	54.5011
6	0.9606	0.9544	1.019	1.11×10^{-6}	263.945
8	0.9770	0.9605	1.033	1.29×10^{-7}	790.305
10	0.9839	0.9645	1.043	1.99×10^{-8}	2169.01
12	0.9814	0.9417	1.032	9.15×10^{-9}	4040.75
14	0.9842	0.9875	1.049	2.81×10^{-9}	8944.68

Table 3: Comparison of present and previous work for various results of $f''(0)$ and $g'(0)$ when $\Pr = 0.72$, $\delta = \varepsilon = Ec = 0.5$, $Mn = f_w = 0$, $\theta_r \to \infty$.

		$f''(0)$			$-g'(0)$		
α	$-S$	Fang and Tao (2012)	Rashidi *et al.* (2014)	Present	Fang and Tao (2012)	Rashidi *et al.* (2014)	Present
0	0.1	0.530	0.530	0.530	0.578	0.578	0.578
	0.2	0.551	0.552	0.551	0.541	0.541	0.541
	0.5	0.614	0.614	0.614	0.428	0.428	0.428
	1	0.719	0.719	0.719	0.236	0.236	0.236
2	0.1	3.117	3.117	3.119	2.053	2.052	2.052
	0.2	3.078	3.078	3.078	2.037	2.037	2.037
	0.5	2.960	2.960	2.960	1.990	1.990	1.990
	1	2.762	2.762	2.762	1.911	1.910	1.910

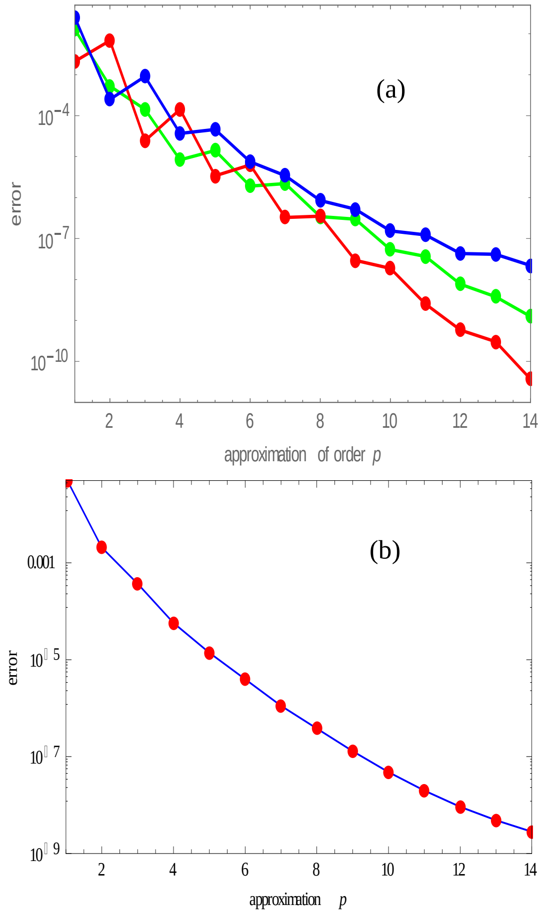

Fig. 2: Residual errors vs order of approximation p (a) Individual residual errors, (b)Total residual error.

IV. VALIDATION OF THE METHODOLOGY

The main purpose of this section is to provide the liability of the current method utilized in the present article. Consider the case $= Mn = S = 1$, $\delta = Ec = 0.5$, $\Pr = 0.72$, $f_w = \varepsilon = 0.1$, $\theta_r = -10$. The 14$^{\text{th}}$ order of approximation is obtained, and the corresponding convergence control parameters are $\bar{h}_f = -0.984215$, $\bar{h}_g = -0.987565$ and $\bar{h}_\theta = -1.04934$, and it is observed that the residual error of each governing equation reduces as we increase the order of approximation (see in Fig. 2(a-b)). Further, Table 3 discussed for the assurance of the OHAM technique, the results are compared with Fang and Tao (2012) and Rashidi *et al.* (2014) and found to be in an excellent manner.

V. RESULTS AND DISCUSSIONS

The main objective of this section is to discuss the influence of various parameters on the flow field with the help of the numerical results. The impact of parameters such as unsteady parameter S, viscosity parameter θ_r, disk stretching parameter α, mass suction/injection parameter f_w, Hartmann number Mn, variable thermal conductivity parameter ε, Prandtl number Pr, Eckert number Ec and Biot number δ on the local Skin friction $f''(0)$ and $g'(0)$ and Nusselt number $\theta'(0)$ is presented in Table.4.

An increase in θ_r, Mn and variations of mass suction/ injection parameter such as $f_w < 0$, $f_w = 0$, $f_w > 0$ results in the decrease of $f''(0)$ and $g'(0)$ and an increase in $\theta'(0)$. This is because $\theta_r \propto 1/\Delta T$, as θ_r rises temperature difference becomes small which leads to the increment in the temperature gradient, and also, in the case of Mn, the result is due to the existence of a magnetic field which creates a Lorenz's force, which opposes the fluid flow. This resisting force slows down the velocity of the fluid. Further, it is noticed that for larger values of the unsteady parameter S, the reduction in the Skin friction, as well as temperature gradient, is recorded. Further, $f''(0)$ and $g'(0)$ are the increasing function of , this is because an increase in the stretching parameter creates more pressure on fluid flow, which leads to an enhancement in the values of $f''(0)$ and $g'(0)$. Concerning Pr we can conclude that the larger values of this parameter results in the reduction of the thermal boundary layer thickness and hence reduced values of $\theta'(0)$ is recorded. In the case of δ, Ec and ε the results are opposite to that of Pr and is due to thermal conductivity $K(T) = k_\infty[1 + \varepsilon\Delta T^{-1}(T - T_\infty)]$ which boosts the temperature gradient.

VI. CONCLUSIONS

In the present article, unsteady MHD flow over an erratic rotating disk with variable fluid properties, mass suction/ injection parameter, viscous dissipation parameter, and convective boundary condition is investigated. Some of the important conclusions are made as follows,

- The unsteady parameter lessens local Skin friction and Nusselt number.
- Fluid viscosity and Hartmann number opposes the fluid flow and strengthened the temperature and exactly opposite characteristics are seen in the case of stretching parameter.

- $f''(0)$ and $g'(0)$ are inversely related with respect to the suction and injection parameter.
- The temperature of the fluid increases with raising the values of variable thermal conductivity, Biot number, and viscous dissipation parameter, whereas inverse impact is seen wit Prandtl number.
- For various values of the unsteady parameter, fluid viscosity, and Hartmann number reduce the skin friction, and the inverse trend is recorded in the case of stretching parameter.
- Impact of viscous dissipation parameter and Prandtl number on temperature gradient is quite opposite.

ACKNOWLEDGMENTS

The authors appreciate the constructive comments of the reviewers which led to definite improvement in the paper.

REFERENCES

Abdul Maleque, K., and Abdul Sattar, M. (2005). "The effects of variable properties and hall current on steady MHD laminar convective fluid flow due to a porous rotating disk," *International Journal of Heat and Mass Transfer.*, **48**, 4963-4972.

Ali, M.E. (1995). "On thermal boundary layer on a power law stretched surface with suction or injection," *International Journal of Heat and Fluid Flow.*, **16**, 280-290.

Amanulla, C.H.,Wakif, A., Boulahia, Z., Suryanarayana Reddy. M. and Nagendra, N. (2018). "Numerical investigations on magnetic field modeling for Carreauo non-Newtonian fluid flow past an isothermal sphere," *Journal of the Brazilian Society of Mathematical Science and Engineering,* **40,** 462.

Chen, C.K. and Char, M. (1988). "Heat transfer of a continuous stretching sheet with suction or injection," *Journal of Mathematical Analysis and Applications,* **135**, 568-580.

Cochran, W.G. (1931)."The Flow Due to a Rotating Disk," *Mathematical Proceedings of the Cambridge Philosophical Society.,* **30**, 365-375.

Cortell, R. (2005). "Flow and heat transfer of a fluid through a porous medium over a stretching surface with internal heat generation/absorption and suction/blowing," *Fluid Dynamics Research,* **37**, 231-245.

Erikson, L.E., Fan, L.T., and Fox, V.G. (1966). "Heat and mass transfer on a moving continuous flat plate with suction or injection," *Industrial Engineering Chemical,* **5**, 19-25.

Fang, T. and Tao, H. (2012). "Unsteady viscous flow over a rotating stretchable disk with deceleration," *Communication in Non linear Science and Numerical Simulation,* **17**, 5064-5072.

Fox, V.G., Erikson, L.E. and Fan, L.T. (1968). "Methods for solving the boundary layer equations for moving continuous flat surface with suction and injection," *Journal of American Institute Chemical Engineering.,* **14**, 726-736.

Fresteri, F. and Osalusi, E. (2007). "On MHD and slip flow over a rotating disk with variable properties," *International Journal of Communication in Heat and Mass Transfer.,* **34**, 495-501.

Gupta, P.S. and Gupta, A.H. (1977). "Heat and mass transfer on a stretching sheet with suction or blowing," *Canadian Journal of Chemical Engineering.,* **55**, 744-746.

Hobiny, A., Ahmed, B., Alsaedi, A., Jalil, M. and Asghar, S. (2015). "Similarity solution for follow over an unsteady nonlinearly stretching rotating disk," *AIP Advances*, **5**, 047113.

Khan, K.A., Butt, A.R. and Raza, N. (2018)." Effects of heat and mass transfer on unsteady boundary layer flow of a chemical reacting Casson fluid," *Results in Physics.,* **8**, 610-620.

Kuiken, H.K. (1971). "The effect of normal blowing on the flow near a rotating disk of infinite extent," *Journal of Fluid Mechanics,* **47**, 789-798.

Liao, S. (2010). "An optimal homotopy-analysis approach for strongly nonlinear differential equations," *Communication in Nonlinear Science and Numerical Simulation.,* **15**, 2003–2016.

Maleki, H., Safaei, M.R., Abdullah, Alrashid, A.A.A., and Kasaeian, A. (2019a). "Flow and heat transfer in non-Newtonian nanofluids over porous surfaces," *Journal of Thermal Analysis and Calorimetry,* **135**, 1655-1666.

Maleki, H., Safaei, M.R., Togun, H. and Daheri, M. (2019b). "Heat transfer and fluid flow of pseudo-plastic nanofluid over a moving permeable plate with viscous dissipation and heat absorption/generation," *Journal of Thermal Analysis and Calorimetry.,* **135**, 1643-1654.

Prasad, K.V. and Vajravelu, K. (2009). "Heat transfer in the MHD flow of a power law fluid over a non-isothermal stretching sheet," *Int. J. Heat mass transfer,* **52**, 4956-4965.

Prasad, K.V., Vaidya, H., Vajravelu, K. and Rashidi, M. (2017a). "Effects of Variable Fluid Properties on MHD Flow and Heat Transfer over a Stretching Sheet with Variable Thickness," *Journal of Mechanics*, **33**, 501-512.

Prasad, K.V., Vajravelu, K., Vaidya, H. and Van Gorder, R.A. (2017b). " MHD flow and heat transfer in a nanofluid over a slender elastic sheet variable thickness," *Results in Physics.*, **7**, 1462-1474.

Prasad, K.V., Vajravelu, K., Vaidya, H., Rashidi, M.M. and Basha, N.Z. (2018). "Flow and heat transfer of a Casson liquid over a vertical stretching surface: optimal solution," *American journal of Heat and Mass Transfer.,* **5**, 1-22.

Prasad, K.V., Vaidya, H., Makinde, O.D. and Srikantha Setty, B. (2019). "MHD mixed convective flow of Casson nanofluid over a slender rotating disk with source/sink and partial slip effects," *Defect and Diffusion Forum.,* **392**, 92-122.

Qasim, M., Wakif, A., Ali, Z. and Boulahia, Z. (2019a). "Numerical simulation of MHD peristaltic flow with variable electrical conductivity and Joule dissipation using generalized differential quadrature method," *Communication in Theoretical Physics* , **71,** 509-518.

Qasim, M., Wakif, A., Afridi, M.I., Nguyen Thoi, T. and Hussanan, A. (2019b). "Second law Analysis of unsteady MHD Viscous flow over a horizontal stretching sheet heated non-uniform in the presence of Ohmic heating: Utilization of Gear- generalized different quadrature method," *Entropy,* **21,** DOI:10.3390/e21030240.

Qasim, M., Wakif, A., Afridi, M.I. and Saleem, S. (2019c). " Influence of Variable transport properties on nonlinear radioactive Jeffery fluid flow over a disk: Utilization of generalized differential quadrature method," *Arabian Journal for Sciene and engineering,* 44, 5987-5996.

Rashidi, M.M., Ali, M., Freidoonimehr, N. and Nazari, F. (2013). "Parametric analysis and optimization of entropy generation in unsteady MHD flow over a stretching rotating disk using artificial neural network and particle swarm optimization algorithm," *Energy,* **55**, 497-510.

Rashidi, M.M., Kavyani, N. and Abelman, S. (2014). "Investigation of entropy generation in MHD and slip flow over a rotating porous disk with variable properties," *International Journal Heat and Mass Transfer.,***70**, 892-917.

Shakiba, A. and Rahimi, A.B. (2019). "Nanofluid flow and MHD mixed convection inside a vertical annulus with moving walls and transpiration considering the effect of Brownian motion and shape factor," *Journal of Thermal Analysis and Calorimetry.,* **137**, 1-15.

Takhar, H.S., Agarwal, R.S., Bhargava, R. and Soundalgekar, V.M. (1995). "Flow of a micropolar fluid past a decelerating porous rotating disk," *International Journal of Nonlinear Mechanics.,* **30**, 295-304.

Turkyilmazoglu, M. (2018). "Fluid flow and heat transfer over a rotating vertically moving disk," *Physics of fluids.,* **30**, 063605.

Vajravelu, K., Prasad, K.V. and Ng, C.-O. (2013). "Unsteady convective boundary layer flow of a viscous fluid at a vertical surface with variable fluid properties," *Nonlinear analysis of Real world applications.,* **14**, 455-464.

Vajravelu, K., Prasad, K.V., Ng, C.-O. and Vaidya, H. (2016). "MHD squeeze flow and heat transfer of a nanofluid between parallel disks with variable fluid properties and transpiration," *International Journal of Mechanical and Material Engineering.,* **6**, 2014-2019.

Van Gorder, R.A. (2019). "Optimal homotopy analysis and control of error for implicitly defined fully nonlinear differential equations," *Numerical Algorithms.,* **81**, 181-196.

Von Karman, T.V. (1921). "Uber Laminare and Turbulente Reibung," *Zeitschriftfür Angewandte Mathematik und Mechanik,* **1**, 232-252.

Wakif, A., Boulahia, Z., Farhad Ali., Eid, M.R. and Sehaqui, R. (2018). " Numerical analysis of the unsteady natural convection MHD Couette Nanofluid flow in the presence of thermal radiation using single and two-phase nanofluid models for Cu-water nanofluids," *International Journal of Applied and Computation Mathematics,* **4,** 81.

Wakif, A., Qasim, M., Afridi, M.I., Saleem, S. and Al-Qani, M.M. (2019a). "Numerical examination of the entropic energy harvesting in a Magnetohydrodynamic dissipative flow of Stokes second problem: Utilization of the gear-generalized differential quadrature method," *Journal of non-Equilibrium Thermodynamics,* **44,** https:/doi.org/10.1515/jnet-2018-0099.

Wakif, A., Boulahia, Z., Amine, A., Animasaum, I.L., Afridi, M.I., Quasid, M. and Sehaqui, R. (2019b). "Magneto-Convection of Alumina-water nanofluid within thin horizontal layers using the revised generalized Boungiorno's model," *Frontiers in Heat and Mass Transfer,* **12,** 3.

Watson, L.T. and Wang, C.Y. (1979). "Deceleration of a rotating disk," *Physics of fluids,*. **22**, 2267-2269.

Watson, L.T., Sankara, K.S. and Luegina, C.M. (1985). "Deceleration of a porous rotating disk in a viscous fluid," *Internal Journal of Engineering Science.,* **23**, 131-137.

Received: October 10, 2019
Sent to Subject Editor: December 20, 2019
Accepted: February 12, 2020
Recommended by Subject Editor: Gianfranco Caruso

Table 4: Values of local Skin friction, Nusselt number, convergence control parameter and average squared residual error for different physical parameters.

Ec	δ	θ_r	Pr	ε	Mn	f_w	S	α	$-f''(0)$	$-\hbar_f$	E_{10}^{f}	$-g'(0)$	$-\hbar_g$	E_{10}^{g}	$-\theta'(0)$	$-\hbar_\theta$	E_{10}^{θ}	CPU Time(sec)
0.5	0.5	-10	0.72	0.1	1	**0.1**	1	**0.5**	4.50838	0.64106	2.26×10^{-4}	2.65815	0.68663	2.84×10^{-4}	0.08706	0.68253	8.26×10^{-5}	1789.5
								1	1.74409	0.93319	1.31×10^{-6}	2.12695	1.01168	2.97×10^{-7}	0.20151	1.03017	3.48×10^{-6}	2527.4
								2	0.64828	1.12736	8.29×10^{-8}	1.83289	1.10466	7.82×10^{-8}	0.24348	1.23999	7.32×10^{-8}	1759.8
0.5	0.5	-10	0.72	0.1	1	**0.1**	**1**	1	1.74409	0.93319	1.31×10^{-6}	2.12695	1.01168	2.97×10^{-7}	0.20151	1.03017	3.48×10^{-6}	2527.4
							2		1.95743	0.80011	8.22×10^{-7}	2.30457	0.82876	8.41×10^{-7}	0.22997	0.87681	1.62×10^{-6}	2013.5
							3		2.15436	0.69615	2.83×10^{-6}	2.47280	0.74192	3.82×10^{-6}	0.24832	0.79265	4.61×10^{-6}	1849.5
0.5	0.5	-10	0.72	0.1	1	**-0.1**	1	1	1.52732	1.03228	3.59×10^{-7}	1.92456	1.00826	2.02×10^{-7}	0.20239	1.09012	2.94×10^{-6}	1846.5
						0			1.63241	0.99685	3.42×10^{-7}	2.02299	0.98864	4.56×10^{-6}	0.20195	1.07423	1.98×10^{-6}	1861.5
						0.1			1.74409	0.93319	1.31×10^{-7}	2.12695	1.01168	2.97×10^{-7}	0.20151	1.03017	3.48×10^{-6}	2527.4
0.5	0.5	-10	0.72	0.1	**1**	0.1	1	1	1.74409	0.93319	1.31×10^{-6}	2.12695	1.01168	2.97×10^{-7}	0.20152	1.03017	3.48×10^{-6}	2527.3
					1.5				1.92585	0.82858	1.75×10^{-6}	2.25486	0.96582	1.58×10^{-6}	0.19025	0.98952	2.74×10^{-6}	2805.2
					2				2.04252	0.75454	2.72×10^{-6}	2.37708	0.81302	8.41×10^{-6}	0.17197	0.85752	4.98×10^{-6}	3092.5
0.5	0.5	-10	0.72	**0.1**	1	0.1	0.5	0.5	0.57351	1.2574	1.11×10^{-7}	1.72308	1.22691	3.64×10^{-7}	0.21911	1.36116	7.28×10^{-6}	1902.5
				0.3					0.57363	1.25936	1.06×10^{-7}	1.72352	1.22691	4.05×10^{-7}	0.21564	1.33647	8.63×10^{-6}	1864.5
				0.5					0.57376	1.26102	1.03×10^{-7}	1.72394	1.22734	4.45×10^{-7}	0.21236	1.31163	8.37×10^{-6}	1953.9
0.5	0.5	-10	**1.09**	0.1	1	0.1	1	1	0.56571	1.23216	1.81×10^{-7}	1.70159	1.22864	3.41×10^{-8}	0.34455	1.27251	1.55×10^{-9}	1965.4
			2						0.56348	1.18879	2.25×10^{-7}	1.69524	1.23198	2.37×10^{-8}	0.38148	1.16059	3.81×10^{-8}	1799.5
			5.09						0.55985	0.87477	8.21×10^{-7}	1.68525	0.83882	8.09×10^{-6}	0.42447	0.68886	1.51×10^{-7}	1810.5
0.5	0.5	**-10**	0.72	0.1	1	0.1	1	1	0.64167	1.12470	9.71×10^{-8}	1.81567	1.10578	9.73×10^{-9}	0.33501	1.26005	2.12×10^{-8}	1889.7
		-5							0.65541	1.13888	8.21×10^{-8}	1.85126	1.10591	1.89×10^{-8}	0.33485	1.26843	2.23×10^{-8}	1881.5
		-2							0.69337	1.17916	5.13×10^{-8}	1.94967	1.13559	8.51×10^{-8}	0.33442	1.29273	2.48×10^{-8}	1839.2
0.5	**0.5**	**-10**	0.72	0.1	1	0.1	1	1	0.56571	1.23216	1.81×10^{-7}	1.70159	1.22864	3.41×10^{-8}	0.34455	1.27251	1.55×10^{-9}	1965.4
	1								0.57207	1.23858	1.81×10^{-7}	1.71876	1.23556	3.11×10^{-8}	0.31453	1.29395	5.74×10^{-9}	1946.4
	2								0.58027	1.23948	1.75×10^{-7}	1.72576	1.24256	2.98×10^{-8}	0.24845	1.31395	3.74×10^{-9}	1956.2
0.5	0.5	-10	0.72	0.1	1	0.1	1	1	0.57351	1.25740	1.11×10^{-7}	1.72308	1.22691	3.64×10^{-7}	0.21911	1.36116	7.28×10^{-6}	1902.5
1									0.57959	1.28798	6.71×10^{-8}	1.73982	1.23648	7.88×10^{-7}	0.12141	1.346422	2.12×10^{-5}	1909.1
1.5									0.58259	1.27858	7.15×10^{-8}	1.74325	1.24245	1.21×10^{-7}	0.82548	1.31254	1.26×10^{-5}	1925.5